Modeling the Wetting Effects in Droplet Impingement using Particle Method

Heng Xie[1], Seiichi Koshizuka[2] and Yoshiaki Oka[2]

Abstract: A model of a single liquid drop colliding on solid surface is developed based with Moving Particle Semi-implicit (MPS) method. The mathematical model involves gravity, viscosity and surface tension. The wettability between the impact liquid and the solid surface is modeled by the contact angle model and the non-slip boundary condition. The particles of the drop are divided into four types in which the model varies to simulate the liquid particles in different area. The model is validated by the comparison of the theoretical results. The complete dynamic process including the spreading, the recoiling, re-bouncing and splashing is simulated and analyzed. It is found that the contact angle plays an important role in the dynamic processes after impact. The impact drop is likely to recoil and rebounce from the surface in the cases of high contact angle so that the critical Weber number for break up varies in different liquid and boundary condition.

Keyword: Droplet impingement; Spreading, Splashing, Particle method, MPS method, Contact angle

1 Introduction

Characteristics of liquid droplet impinging on surface are of great importance in many technical applications including spray coating, pesticide applicant, ink-jet painting and spray cooling. This process is also encountered in nuclear engineering. In LWR (Light Water Reactor), liquid droplet

behaviors are related to core thermal-hydraulics: such as the mist-annular flow existing in BWR (Boiling Water Reactor) and the dispersed droplet flow in post-CHF regime. In the former, the mechanism of the droplet impacting on the liquid film attached on the surface of fuel rod will affect the deposition of droplet and subsequently the mass flux and thickness of the liquid film which are key parameters of dry-out phenomena. In the latter, the direct contact between liquid droplets and the wall has an important contribution to the heat transfer [Guo and Mishima (2002), Cokmez et al (2000)].

The study of droplet impact dynamic has received attention from researchers for more than one century [Worthington (1877)]. The review by Rein (1993) summarized important aspects of the impact process. In recent years, photographic images were used to observe the features of droplet impact [Fukai et al (1995), Zhao et al (1996b), Bussmann et al (1999, 2000), Kang and Lee (2000), Kim and Chun (2001), Šikalo et al (2002), Zapałowicz (2002), Riboo et al (2002)]. The impact process was divided into two distinct stages from these results: spreading and recoiling stages. A droplet immediately spreads after impact on the solid surface; when the contact area reached the maximum value, it recoiled, and even rebounded from the surface. The splashing also occurred in some cases. The phenomena are extremely complex, for a number of factors including initial droplet velocity, droplet size, liquid viscosity, surface tension and wetting effects etc. affect the process. The present knowledge of the droplet impact dynamic is far from complete.

Many numerical simulations have been carried out in order to understand the characteristics of the impact dynamics. The complexity of the dynamics makes it difficult to simulate. There are

[1] Corresponding Author. 103Divison, Energy Science Building, Institute of Nuclear Energy Technology, Tsinghua University, Beijing 100084, P.R.China. Tel: +86-10-6278-3555, Fax: +86-10-6277-1150, Email: xieheng@mail.tsinghua.edu.cn
[2] Nuclear Engineering Research Laboratory, The University of Tokyo, Japan

several reasons. Break up as well as large deformation of the droplet surface occurs within a very short time scale. The exact numerical model for wettablity is another difficulty for simulation.

Harlow and Shannon (1967) used "marker in cell" (MAC) [Harlow and Welch, (1965)] finite difference technique based on fix grid, where viscous, surface tension and wettability were neglected. Trapaga and Szekely (1991) used the commercial code FLOW-3D that employs a fixed grid Eulerian approach in conjunction with "volume of fluid" (VOF) [Hirt and Nichols (1981)] method to track the droplet surface. Surface tension and contact angle models were included. The VOF method has also been used by other researchers to simulate the drop impact problem. [Liu et al (1993), Fukai et al. (1993, 1995, 1997), Zhao et al. (1996a), Tong and Holt (1997), Pasandideh_Fard et al (1998), Bussmann et al (1999, 2000)]. Kinematic discontinuities theory was employed by Yarin and Weiss (1995) Trujillo and Lee (2001) to simulate the crown formed after impact. Zhang and Yabe (1999) used the "Cubic-Interpolated propagation" (CIP) method to study the breakup in crown formation and the effect of ambient gas. Reznik and Yarin (2002) used "Boundary Element Method"(BEM) to study the spreading of drop on dry wall.

In recent years, meshless methods had been more and more widely applied in the simulation of solid mechanics, such as Meshless Local Petrov-Galerkin (MLPG) method (Andreaus et al. 2005, Sladek et al. 2006, Atluri et al. 2006, Ching and Chen 2006) and material point method (Tang et al. 2003, Bardenhagen and Kober 2004, Guo and Nairn 2006, Ma et al. 2006). In the area of fluid mechanics, meshless particle method had been developed due to its characteristic in simulation of some complex flow. To simulate large deformation of free surface, particle method has a natural advantage, it is not necessary to use grids or VOF function to track the free surface. Numerical diffusion can be avoided since the convection is directly calculated by the motion of particles. In the present study the wetting effects, which is represented by advancing and receding contact angle, is developed and enhanced to Moving-Particle Semi-implicit (MPS) method. Then the complete dynamics process of liquid droplet impact on solid surface is simulated and analyzed.

2 Mathematical model

2.1 Governing equations

Mass and momentum conservation equations for incompressible flows are shown as follows:

$$\frac{D\rho}{Dt} = 0 \tag{1}$$

$$\rho \frac{D\mathbf{u}}{Dt} = -\nabla P + \eta \nabla^2 \mathbf{u} + \rho g + \sigma \kappa \delta \mathbf{n} \tag{2}$$

where ρ is density, $\mathbf{u}$ is velocity, t is time, P is pressure, η is viscosity, g is gravitational acceleration, σ is surface tension coefficient, κ is curvature of the surface, δ is the delta function, $\mathbf{n}$ is the unit vector normal to the surface.

These governing equations involve differential operators, such as gradient and Laplacian. The method to discretize these operators is shown in the next sub-section. Convection terms are not needed to calculate since the MPS method is fully Lagrangian. Thus, numerical diffusion does not occur.

2.2 MPS method

Since the MPS method has been introduced in many published papers, it is described in brief here. The detail of the model and the algorithm can be seen from the references [Koshizuka and Oka (1996), Nomura et al (2001), Xie et al (2004a,2004b,2005)].

In the MPS method a particle interacts with others in its vicinity covered with a weight function $w(r)$, where r is the distance between two particles(Fig.1). In this study, the following function is employed

$$w(r) = \begin{cases} \frac{r_e}{r} - 1 & (r < r_e) \\ 0 & (r > r_e) \end{cases} \tag{3}$$

Since the area that is covered with this weight function is bounded, a particle interacts with a finite number of neighboring particles. The radius
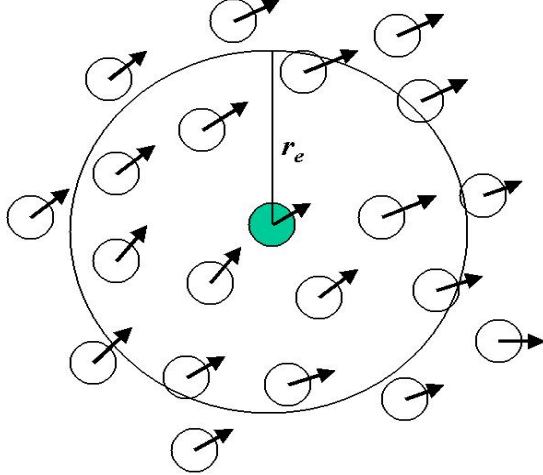
Figure 1: Particle interaction within weight function

of the interaction area is determined by a parameter r_e. The particle number density at co-ordinates $\mathbf{r}_i$ is defined by

$$\langle n \rangle_i = \sum_j w(|\mathbf{r}_j - \mathbf{r}_i|) \tag{4}$$

A gradient vector between two particles i and j possessing scalar quantities ϕ_i and ϕ_j at co-ordinates $\mathbf{r}_i$ and $\mathbf{r}_j$ is simply defined by $(\phi_j - \phi_i)(\mathbf{r}_j - \mathbf{r}_i)/|\mathbf{r}_j - \mathbf{r}_i|^2$. The gradient vector at the particle i is given as the weighted average of these gradient vectors.

$$\langle \nabla \phi \rangle_i = \frac{d}{n^0} \sum_{j \neq i} \left[\frac{\phi_j - \phi_i}{|\mathbf{r}_j - \mathbf{r}_i|^2} (\mathbf{r}_j - \mathbf{r}_i) w(|\mathbf{r}_j - \mathbf{r}_i|) \right] \tag{5}$$

where d is the number of space dimensions and n^0 is the particle number density.

Laplacian is an operator representing diffusion. In the MPS method, diffusion is modeled by distribution of a quantity from a particle to its neighboring particles by use of the weight function as shown in Fig.2:

$$\langle \nabla^2 \phi \rangle_i = \frac{2d}{n^0 \lambda} \sum_{j \neq i} \left[(\phi_j - \phi_i) w(|\mathbf{r}_j - \mathbf{r}_i|) \right] \tag{6}$$

where λ is a parameter by which the variance in-

crease is equal to that of the analytical solution:

$$\lambda = \frac{\sum_{j \neq i} w(|\mathbf{r}_j - \mathbf{r}_i|) \, |\mathbf{r}_j - \mathbf{r}_i|^2}{\sum_{j \neq i} w(|\mathbf{r}_j - \mathbf{r}_i|)} \tag{7}$$
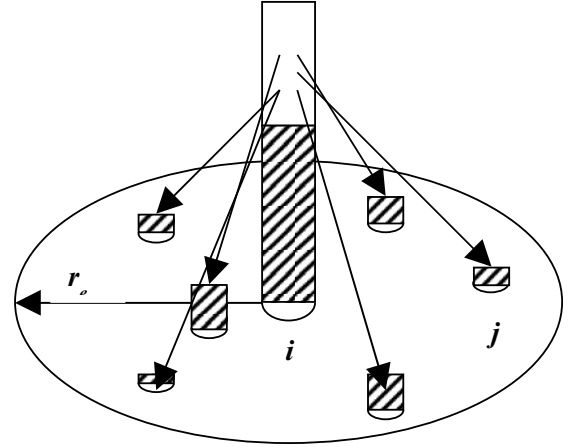

Figure 2: Concept of Laplacian model

Incompressibility is calculated by a semi-implicit algorithm where the pressure field is implicitly solved using the Poisson equation, while the other terms are explicitly calculated,

$$\langle \nabla^2 P \rangle_i = -\frac{\rho}{\Delta t^2} \frac{n_i^* - n^0}{n^0} \tag{8}$$

where superscript * stands for a temporal value after the explicit calculation step. The source term of the Poisson equation is represented by the deviation of the particle number density from the constant value of n^0.

2.3 Discretization of viscosity term

In the momentum conservation equation (Eq.2), the viscosity term has the form of the Laplacian operator. So Eq.6 is adopted for discretization of the viscosity term:

$$\langle \nabla^2 \mathbf{u} \rangle_i = \frac{2d}{n^0 \lambda} \sum_{j \neq i} (\mathbf{u_j} - \mathbf{u_i}) w(|\mathbf{r}_j - \mathbf{r}_i|) \tag{9}$$

The viscosity term is calculated in the explicit step

Viscosity force between a liquid particle and a outside air particle is much smaller than that between liquid particles when the velocity of air is small. Therefore, the outside air is treated as vacuum and no air particles are located.

2.4   Surface tension model

Surface tension is calculated at the particles on the free surface. We need to obtain curvature κ and a unit normal vector $\mathbf{n}$ at such particles (Fig.3). The particle number density is utilized for curvature.

$$\kappa = \frac{2\cos\theta}{r_e^{st}} \tag{10}$$

$$2\theta = \frac{n_i^{st2}}{n_0^{st}}\pi \tag{11}$$

where the weight functions used here are special for surface tension,

$$w^{st1}(r) = \begin{cases} 1 & 0 \le r < r_e^{st} \\ 0 & r_e^{st} \le r \end{cases} \tag{12}$$

$$w^{st2}(r) = \begin{cases} 1 & 0 \le r < r_e^{st} \text{ and } n_j^{st1} > n_i^{st1} \\ 0 & \text{otherwise} \end{cases} \tag{13}$$

and r_e^{st} is the parameter that determines the neighbor in the calculation of surface tension. Particle number density n_i^{st1} is calculated by using Eq.12 at first, and n_i^{st2} is then obtained by using Eq.13.
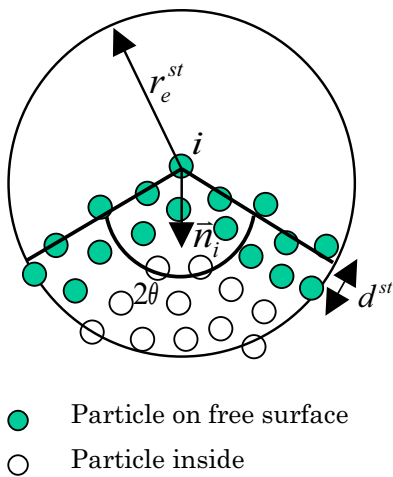

Figure 3: Surface tension model

In Eq.11, a flat surface ($2\theta = \pi$) is assumed to be $n_i^{st2} = n_0^{st}$, which is estimated in advance in the initial particle configuration. Acute angles are obtained where $n_i^{st2} < n_0^{st}$, while obtuse angles are obtained where $n_i^{st2} > n_0^{st}$.

The unit normal vector is also calculated by utilizing the particle number density. Particle number densities at four positions near particle i are evaluated, $n_i^{\pm x}(\mathbf{r}_i \pm l_0\mathbf{n}_x)$ and $n_i^{\pm y}(\mathbf{r}_i \pm l_0\mathbf{n}_y)$ where $\mathbf{n}_x$ and $\mathbf{n}_y$ are unit vectors in x-and y-directions, respectively and l_0 is the spacing between adjacent particles in the initial configuration. The unit normal vector is calculated as,

$$\mathbf{a}_i = \frac{n_i^{+x} - n_i^{-x}}{2l_0}\mathbf{n}_x + \frac{n_i^{+y} - n_i^{-y}}{2l_0}\mathbf{n}_y \tag{14}$$

$$\mathbf{n}_i = \frac{\mathbf{a}_i}{|\mathbf{a}_i|} \tag{15}$$

Vector $\mathbf{a}_i$ represents gradient of the particle number density around particle i. For stability, curvature is smoothed as follow:

$$\kappa_i = (\kappa_i^* + \sum_{j \ne i} w(|\mathbf{r_j} - \mathbf{r}_i|)\kappa_j^*)/2.0 \tag{16}$$

where κ_i^* is the curvature of particle i before smoothing and κ_i is that after smoothing. κ_j^* is the curvature of particle j which is in the neighbor of particle i before smoothing.

As shown in Fig.3, free surface particles have a thickness. Thus, we need to divide the calculated surface tension by the normalized thickness of d^{st}/l_0. This model is based on the distribution of the particle number density because it decreases toward the free surface. This idea is similar to the CSF (Continuum Surface Force) model [Brackbill et al (1992)]. Verification of the surface tension model is shown in Nomura et al (2001).

2.5   Wettability model

Wettability is represented by the contact angle and the non-slip boundary condition. If a small drop of liquid is placed on a uniform, perfectly flat, solid surface, it will, in general, not spread completely over the surface, but its edge will make an angle with the solid, as shown in Fig.4 [Davies et al (1961)]. This angle is the contact angle.
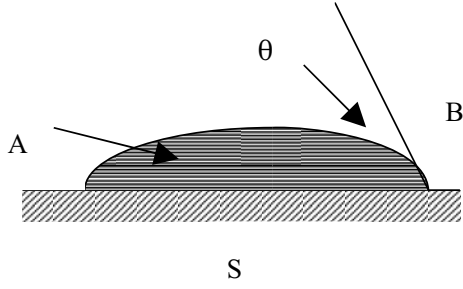
Figure 4: The schematic of contact angle

- ● Boundary particle
- ⊘ Contact line particle
- ⊘ Contact line free particle
- ○ Other particle

Figure 5: Contact angle model

The contact angle of fluid A on solid S can be written in the next equation [Slattery et al (1982)]:

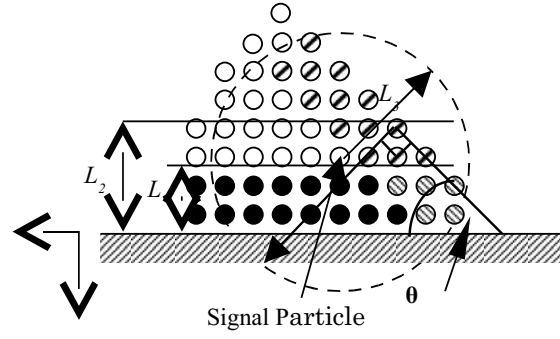$$\cos\theta = \frac{1}{\sigma^{(AB)}}(\sigma^{(BS)} - \sigma^{(AS)}) \qquad (17)$$

where σ is the interface tension between different phases.

The contact angle is affected by the surface material and temperature. These factors will influence the capillary phenomena near the contact line between the solid and the liquid. Normally, a contact angle depends on the motion of the contact line. The contact angles of advance and recede stages are different. The advancing contact angle is always larger than the receding contact angle.

The contact angle also depends on the velocity. This is not so strong if the flow is not dominated by the capillary force, which is the case for most duration of the simulation [Fukai et al (1995)]. Therefore, the constant values are used for the contact angles. Two values are employed for advancing angle and receding angle, respectively, in our calculation.

The calculation method of contact angle is shown in Fig.5. The particles near the contact line are divided into 4 types. The particles near the solid surface are named boundary particles. The boundary particles that are located in the contact line area are named contact line particles. Other particles located in the contact line area are named contact line free particle. Other particles except the above three types of particle are named as other particles.

The type of particles is set by the following three steps.

1). The particles whose distance from the solid surface is less than parameter L_1 are set as boundary particles.

2). The particle satisfying the next three conditions are set as signal particle.

   a. The distance between it and wall is less than parameter L_2 and greater than parameter L_1;

   b. Non-surface particle;

   c. It is located at the most outside of all particles that satisfy the condition a) and b).

3). For the surface particles located at the neighbor of signal particle, the boundary particles are set as contact line particles and the non-boundary particles are set as contact line free particles. Parameter L_3 is the radius of the neighbor of signal particle as shown in Fig.5.

The parameter L_1 and L_2 depend on the thickness of boundary liquid film and the parameter L_3 depends on the size of contact line area. In this calculation, the parameter L_1, L_2 and L_3 are assumed to be $2.1l_0$, $4.1l_0$ and $4.1l_0$ respectively.

The contact angle model is combined with the surface tension model. For the contact line free particles, the unit vector normal to the interface **n** in

Eq.2 is set as

$$\mathbf{n} = \mathbf{n_{wall}} \cos\theta + \mathbf{n_t} \sin\theta \qquad (18)$$

where $\mathbf{n}_{wall}$ is the unit vector normal to the wall, $\mathbf{n_t}$ is the unit lie in the wall and directed into the liquid and θ is the contact angle. Curvature κ is calculated by the same equation as in surface tension model. For the contact line particles, the vector $\mathbf{n}$ is calculated by the same way as the contact line free particles. Since these particles are near the solid surface, calculation of curvature of the surface κ using the particle number density method is not proper. The curvature of the nearest contact line free particle is used instead by assuming the curvature are continuous. For the boundary particles, the calculation method is related to non-slip boundary condition. A thin liquid film in which the liquid particles do not move is assumed on the area near the solid surface. These particles are boundary particles in Fig.5. Non-slip boundary is usually modeled by setting the surface velocity on the solid to be zero. However, in this calculation method the spacing between particles is very small and the thickness of boundary particles layer may be less than that of the thin liquid film. The method mentioned above will not be proper. Therefore, the lateral slip of boundary particles is prohibited to simulate the non-slip boundary.

3   Simulation Results

3.1   Static contact angle

The contact angle is the angle formed between the edge of liquid drop and the solid surface as shown in Fig.4. As an example to verify the present model, static shapes of a liquid droplet attched on the solid surface are simulated. The spacing between adjacent particles l_0 is set to be 0.08mm and 2916 particles are used. The six cases of contact angle 15º, 30º, 45º, 60º, 75º and 90º are simulated. The simulated result of a typical case of contact angle 60º is shown in Fig.6.

When the droplet reach static, the stress balance should make the angle between droplet surface and solid surface approach the contact angle. In Fig.7, the calculated results are compared with the input data. Good agreement are obtained.
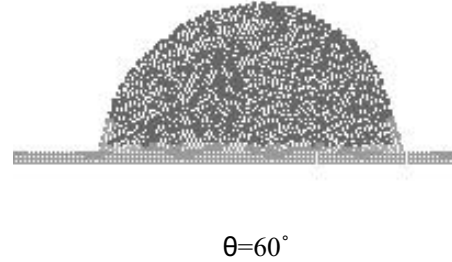

θ=60˚

Figure 6: Static shapes of a droplet attached on the solid surface (θ=60º

3.2   Anvance and recede angle

An experimental method to measure dynamic contact angle for the spreading and recoiling stages of process is tilting the plate that liquid droplet attached on and directly measure the advancing and receding angles just before drop mobilization. The front (leading) contact point measurement provides the advance angle, while the rear (trailing) contact point measurement provides the recede angle (Fig.8). This case is simulated. The incline angle of plate is set to be 45. The spacing between adjacent particles l_0 is set to be 0.1mm and 2500 particles are used to simulate the liquid droplet. Five cases of advance and recede contact angle (120º, 60º), (150º, 30º), (45º, 45º), (90º, 90º) and (135º, 135º) are calculated. The simulated result of case of contact angle (120º, 60º) is shown in Fig.9.

The contact angles obtained from the calculated results should agree with the input data if the simulation succeeds. In Fig.10, it can be seen the calculated results agree well with the input data.

3.3   Comparison with analytical results of droplet impingement

In the work of Roisman et al (2002), a theoretical model for the droplet impingement process was presented. They assumed that the impacting drop consisted of three parts (Fig.11): an undisturbed part moving as a rigid body with pre-impact velocity (region 1), a part in the gap between region 1 and wall, where a high pressure gradient occurs (region 2), and the liquid squeezed as a lamella from region2 (region 3). In region 3, outside the
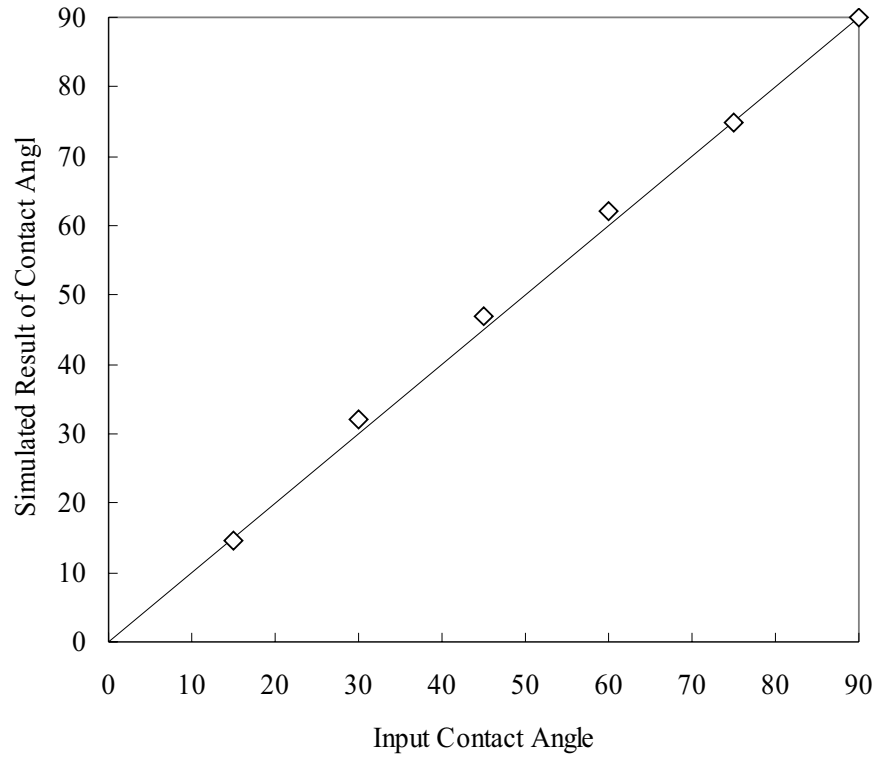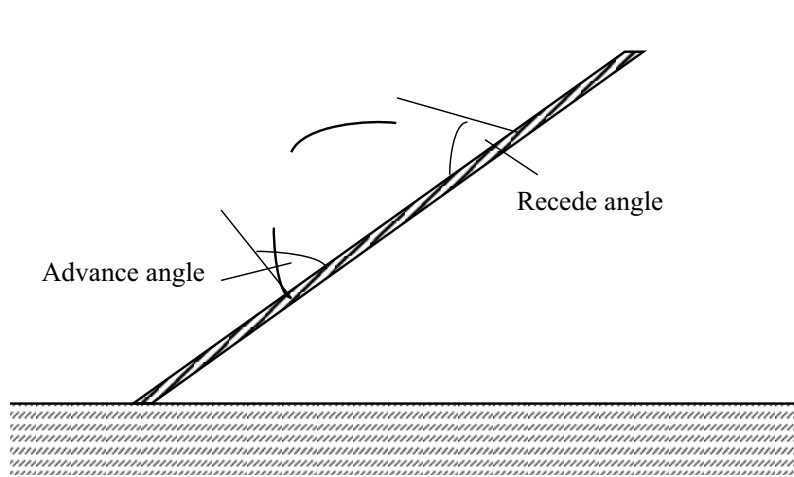
Figure 7: Simulated results of static cases

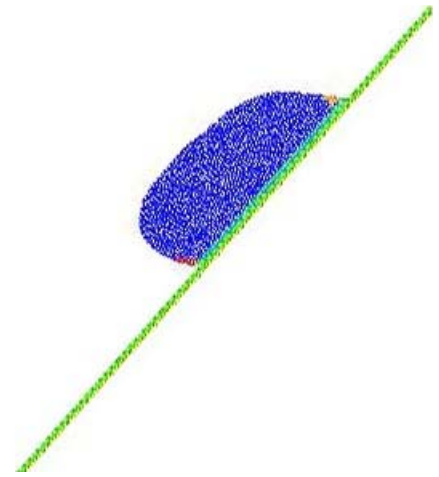Figure 8: Schematic of advance and recede angle

Figure 9: Simulated results of droplet on incline plate

gap between region1 and wall, the velocity gradients are not so high as in region 2 and the pressure was assumed to be uniform. In region 2, the inertial terms in the momentum equation was neglected. Then, a theoretical equation for the dimesionless lamella thickness at the initial phase of impact $\overline{h}_1 = h_1/D_0$ was obtained.

$$3We + 5(1 - \cos\theta)Re\overline{h}_1 = 10ReWe\overline{h}_1^3 \qquad (19)$$

where h_1 is the average thickness of lqiuid lamella formed at the impact process, D_0 is the pre-impact drop diameter, We is Weber number ($We =$
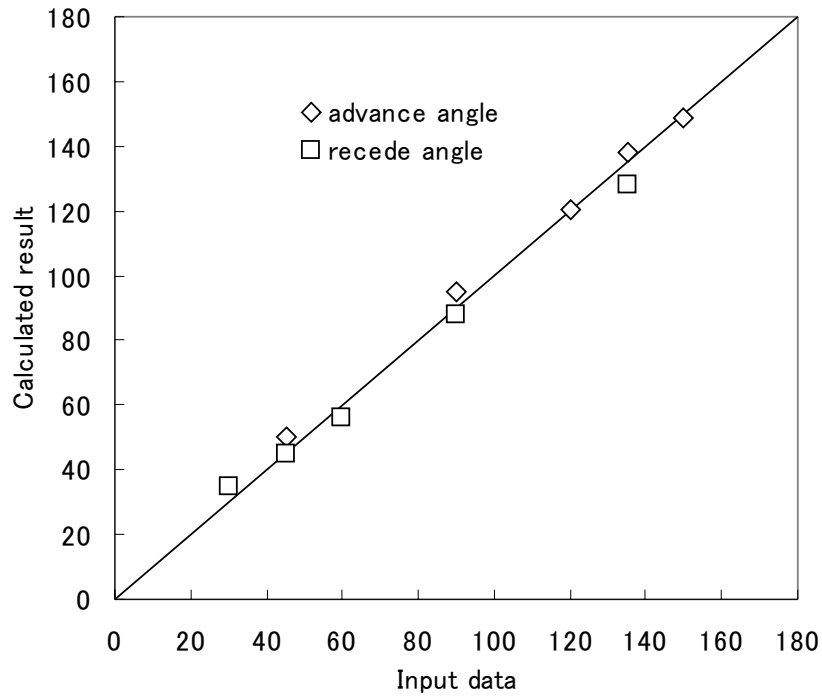
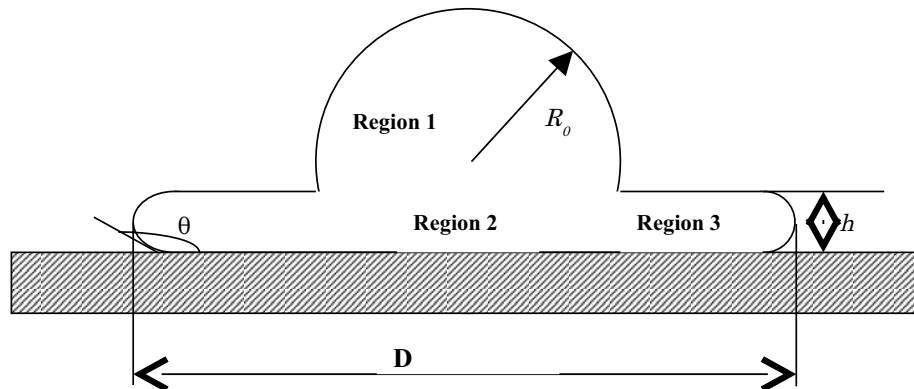Figure 10: Simulation results of advance and recede angle(^{o})

Figure 11: Schematic of drop impact

$\rho U_0^2 D_0/\sigma$, U_0 is pre-impact drop velocity), Re is Reynolds number ($Re = \rho U_0 D_0/\mu$), θ is contact angle.

After solving this equation, a dimensionless drop diameter d_1 at the instant $t = D_0/U_0$ can be obtained:

$$d_1 = \frac{D_1}{D_0} = \sqrt{\frac{2}{3\overline{h}_1}} \qquad (20)$$

where D_1 is the diameter of lamella formed after impact.

Above analytical equations are obtained at the ax-

isymmetrical cylindrical coordinate system. Using the same approximations and method, the theoretical equations in 2D Cartesian coordinates can be gotten:

$$3We + 2(1 - \cos\theta)Re\overline{h}_1 = 4ReWe\overline{h}_1^{-3} \qquad (21)$$

$$d_1 = \frac{D_1}{D_0} = \frac{\pi}{4\overline{h}_1} \qquad (22)$$

To verify the present numerical model, some cases of liquid drop impact on solid surface are simulated. The drop dimater is set as 2mm, 1265 prticles is employed to simulate the drop. Impact

velocity is set as 0.5m/s ($We = 5$, $Re = 10$), 1m/s ($We = 20$, $Re = 20$), 2m/s($We = 80$, $Re = 40$) and 4m/s($We = 320$, $Re = 80$). The contact angle is set as 0°, 60° and 120°.

In Fig.12, the theoretical values of dimensionless diamer d_1 calculated by equations (21) and (22) are compared with simulation results. From the figure, it can be seen that the simulation results approach the analytical results with the decrease of impact velocity. The reason can be explained as follow: In the work of Roisman et al (2002), the inertial term of the momentum equation in region 2 is neglected. This approxiamtion is unreasonable when the impact velocity is big. Therefore, above analytical results are more suitable to the cases of low Weber number and Reynolds number.

To further verify this explanation, the errors between simulation and analytical results of various Weber number and Reynolds number are shown in Fig.13 and Fig.14. From these figures, it can be seen that the errors decreases with the decrease of Reynolds number and Weber number. These figures also show that the simulated values are very close to analytical values in the cases of low Reynolds number and Weber number.

3.4 Simulation of complete process of impingement

To illustrate the complete progress of droplet impact and verify the model described above, two typical cases in Fukai et al.'s experiment (1995) are chosen to simulate. Case A is the case 3 in Fukai et al (1995), a water droplet of radius r_0=1.88mm impinges on a flat glass plate with a velocity of v_0=1.50m/s. Case B is the case 6 in Fukai et al (1995), a water droplet of radius r_0=1.86mm impinges on a flat glass plate with a velocity of 1.58m/s. The droplet parameters of two cases are close. The main difference of these two cases is the surface condition of the plate. Pyrex glass plates with different roughness are used. The contact angles of water on them are measured; the advanced angle is 60° and the recede angle is 22° in case A, and the advanced angle is 92° and the recede angle is 60° in case B. For water at room temperature and pressure, the

following parameters are employed: density $\rho = 1000$kg/m^3, viscosity $\upsilon = 9.7 \times 10^{-7}$m^2/s, and surface tension coefficient $\sigma = 0.073$N/m. The impact Weber number ($We = \rho u^2 D/\sigma$) is 58.4 in case A and 64.1 in case B. A two-dimensional code of the MPS method is used. The coordinates normal and parallel to the solid surface are considered. It is improper to quantitatively compare the simulation results with the experimental results since the circumferential flow is omitted in present two-dimensional model. However, qualitatively analysis is still meaningful since it can help to understand the complete impact process and the effect of wettability. The influence of other factors in impact process can also be studied according to analysis of 2D simulation results.

Similar to mesh resolution independence in mesh method, the particle resolution dependence should be examined first in the particle method. Case A is employed as a test. Three calculations in which the initial spacing between adjacent particles are 0.06mm, 0.08mm and 0.1mm are carried out. The results of the diameter of the contact area on the solid surface are shown in Fig.15. It can be seen that the results of 0.06mm and 0.08mm are close. The case of 0.1mm seems to be inaccurate. The CPU time increases when the spacing is smaller. Therefore, the spacing of 0.08mm is chosen in the following simulations.

The sensitivity test of r_e^{st}, which is the parameter that determines the neighbor in the calculation of surface tension (Eqs 10~13) are carried out. Case A is employed as a test again. Three calculations in which r_e^{st} are $2.1l_0$, $3.1l_0$ and $4.1l_0$ are carried out. The results of the diameter of the contact area on the solid surface are shown in Fig.16. It can be seen that the results of $3.1l_0$ and $4.1l_0$ are close. The case of $2.1l_0$ seems to be inaccurate. In the condition that the free surface is smooth, the results is more accurate when the parameter r_e^{st} is larger. On the other hand, employing larger parameter r_e^{st} will inevitably omit small local curvature change in the surface. Considering these contrary requirements, $r_e^{st} = 3.1l_0$ is employed in this simulation.

The calculated results are shown in Fig.17 and Fig.18 in which the dimensionless time unit $\tau =$
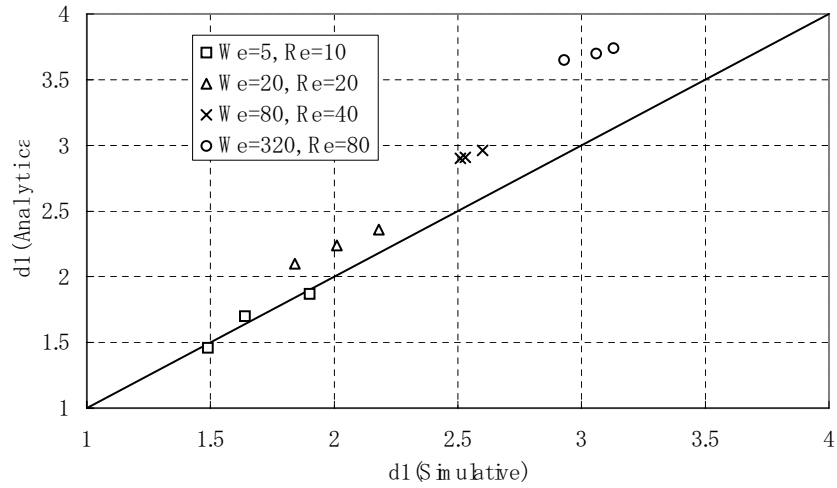
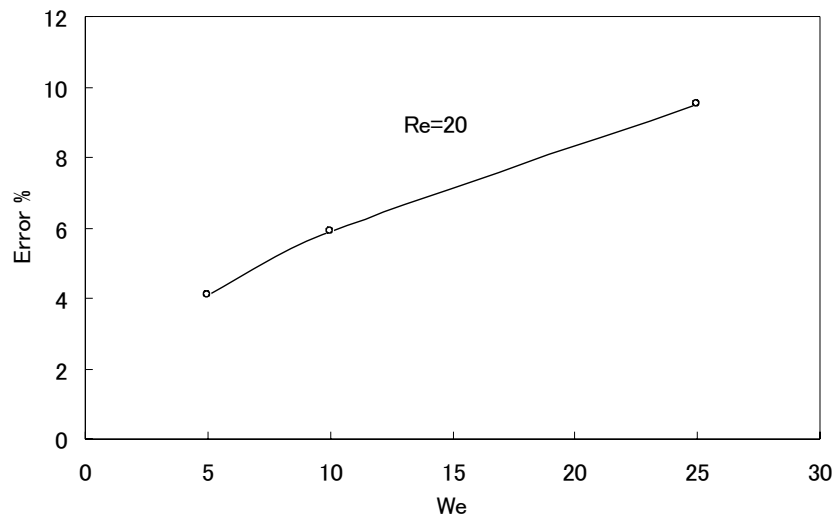Figure 12: The dimensionless diameter of the drop at the time $t = D_0/U_0$.

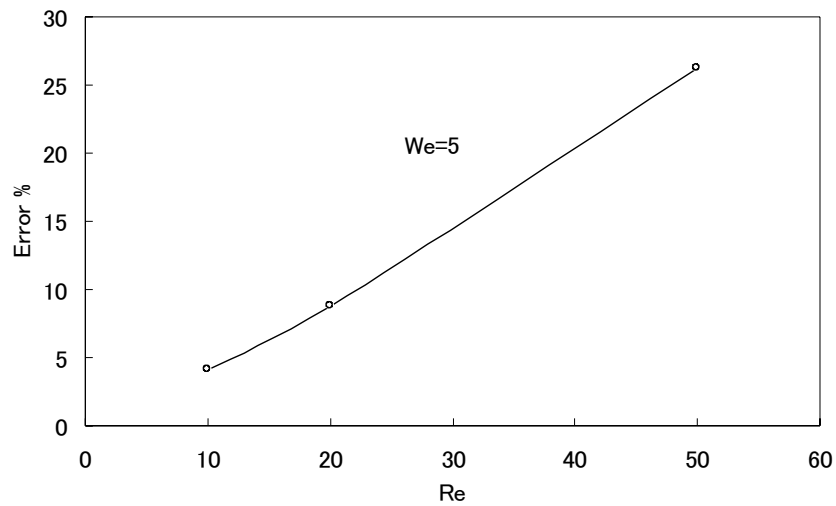Figure 13: The error between analytical and simulated results of various Weber number

Figure 14: The error between analytical and simulated results of various Reynolds number
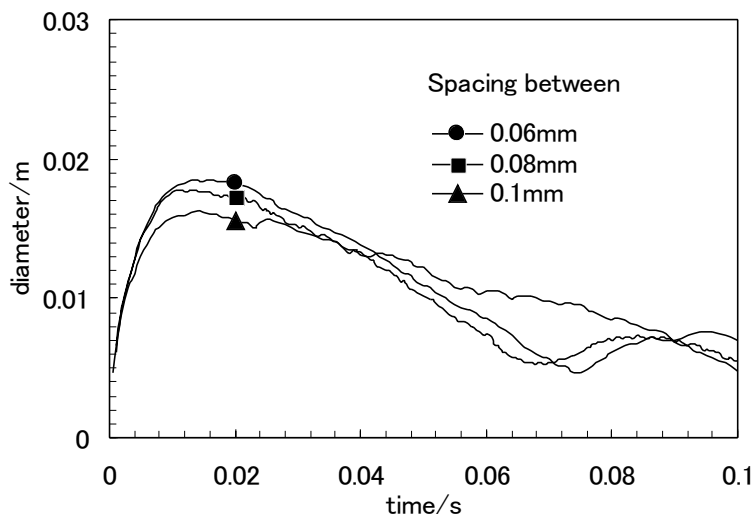
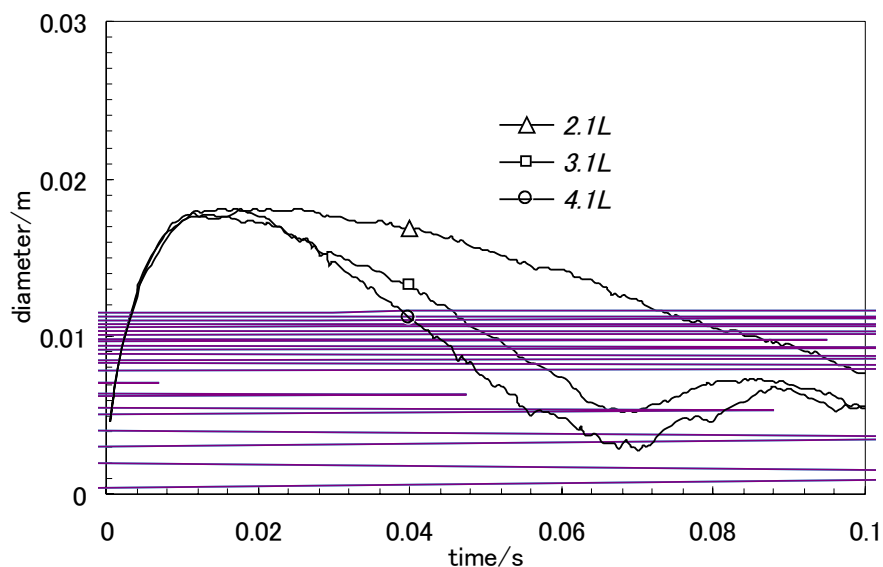Figure 15: Diameter of contact area versus time on different initial spacing between adjacent particles

Figure 16: Diameter of contact area versus time on different parameter r_e^{st}

tv_0/r_0 is employed as in Fukai et al (1995). It can be seen that droplet spreads on the solid surface after impact. With the spreading of the droplet, the pre-impact kinetic energy is transferred to surface energy. Mass accumulated in the contact line area of the periphery of the droplet increases the curvature of the surface and the surface tension. Then the spreading are held up and more mass are accumulated in the contact line area. This further enhances surface tension and the spreading speed becomes slower and slower. When the inertia cannot overcome the viscosity and surface tension, the spreading of the droplet stops. The mass accu-mulation at the periphery of the droplet continues for a short time. When the surface tension is big-ger enough, the recoil stage of the droplet begins. In this stage the surface energy is reverse trans-ferred to inertia and causes the recoil and sub-sequently upward motion. As mentioned above, the main difference of the two cases is the sur-face condition that can be described by the con-tact angle. It is apparent in the Figs.17 and 18 that the bigger contact angle causes stronger re-coil and upward motion. It can be explained as follows. The bigger contact angle causes larger curvature and stronger surface tension at the pe-
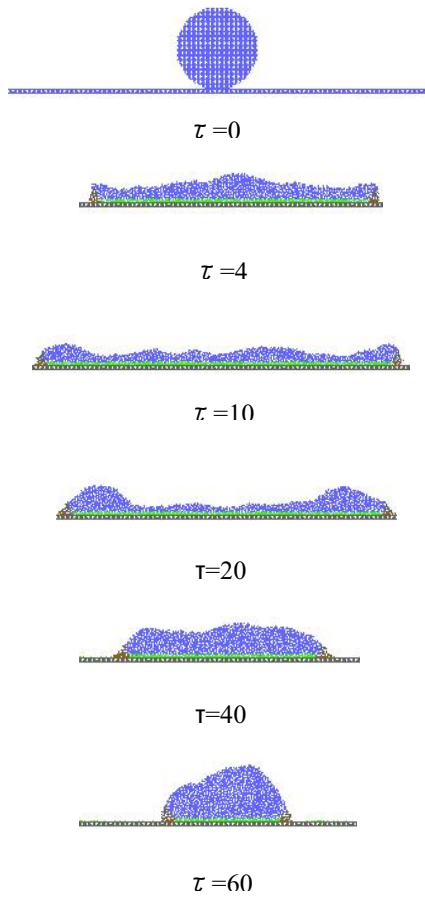
$\tau = 0$

$\tau = 4$

$\tau = 10$

τ=20

τ=40

$\tau = 60$

Figure 17: Calculated sequence of CASE A

$\tau = 0$

$\tau = 4$

$\tau = 10$

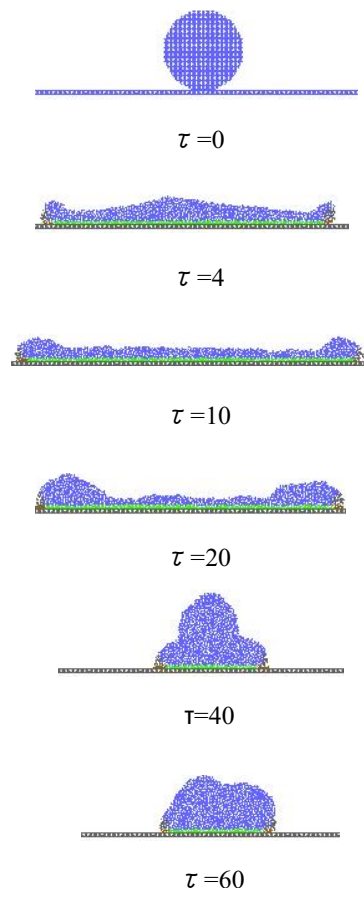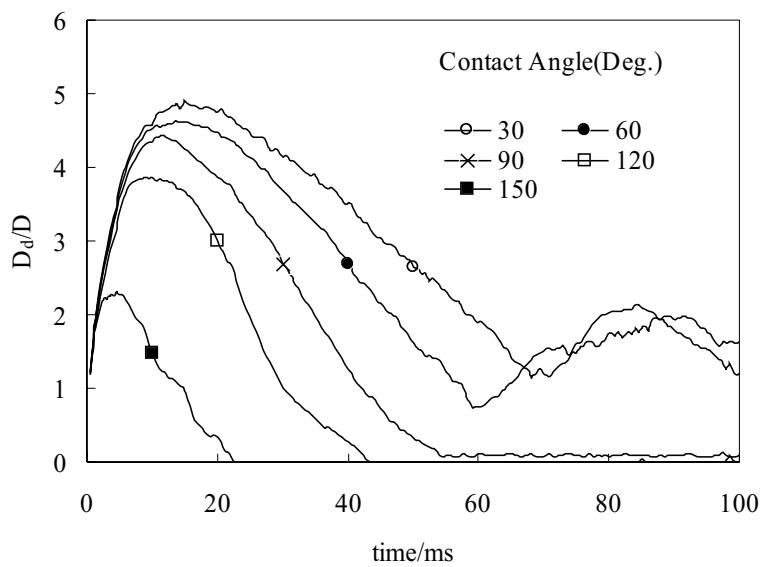$\tau = 20$

τ=40

$\tau = 60$

Figure 18: Calculated sequence of CASE B

Figure 19: The variation of spread factor (*We*=58.4)

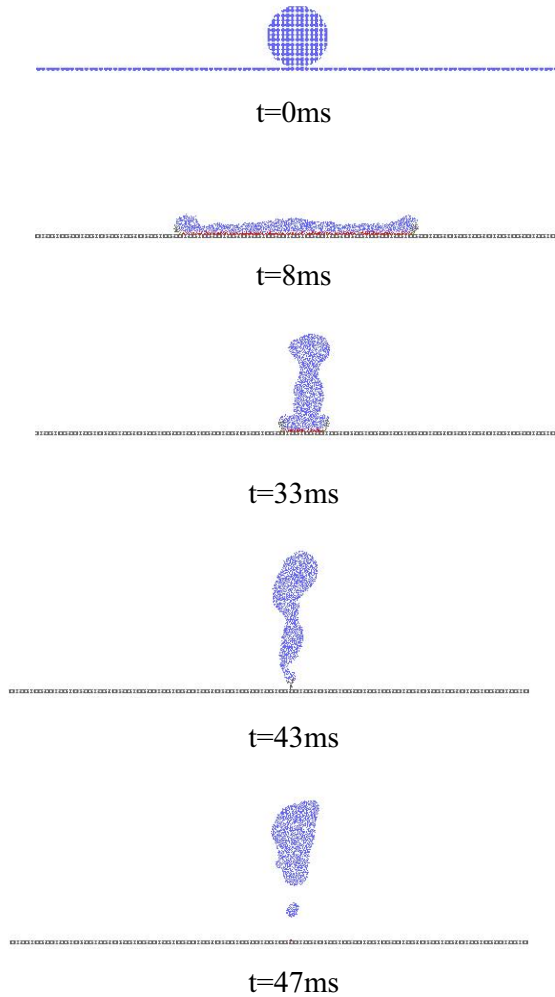Figure 20: Calculated sequence (*We*=58.4, Contact angle θ=120°

Figure 21: Calculated sequence (*We*=58.4, Contact angle θ=150°

riphery of the droplet, and then the spreading of the droplet is decelerated and more mass are accumulated at the periphery. Subsequently larger surface energy causes stronger inward flow and greater upward motion in the recoiling process. The sequence of photographs of case 6 is shown in Fukai et al (1995). The results of our simulation agree with the experimental results.

To study the effect of contact angle on the dynamic process, several cases in which only the contact angle varies are simulated. Five cases based on the droplet parameters of the case A are calculated: contact angles are 30°, 60°, 90°, 120° and 150°. The results of spread factor (D_d/D)(D_d is the diameter of the contact area after impact
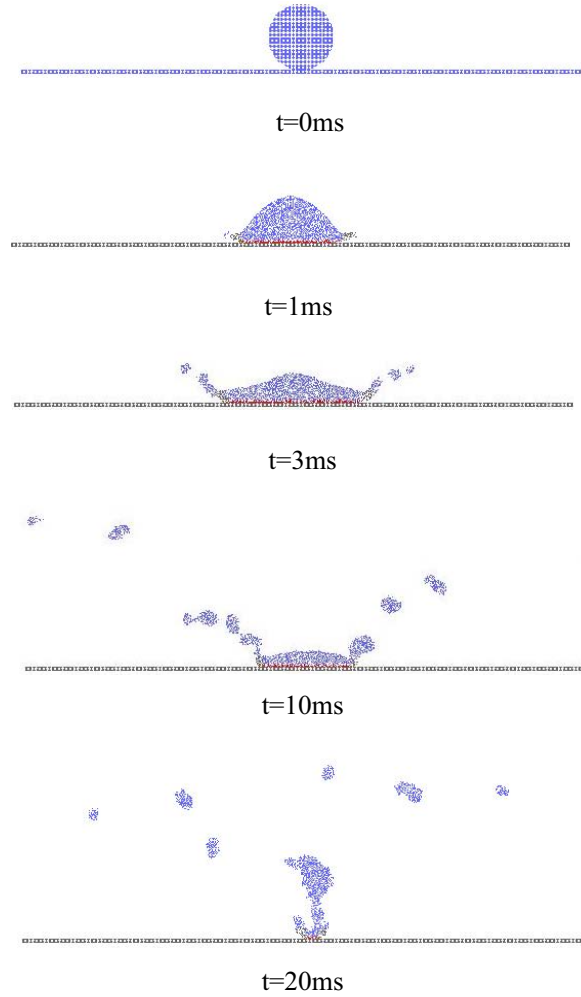
and D is the diameter of pre-impact droplet.) are shown in Fig. 19. In the first stage of spreading, the surface condition has slight effect on the spreading velocity as shown in the experiment of Riboo et al (2002). The reason is that the inertia plays the most important role in this stage. Then the effect of contact angle becomes important. The maximum spread factor increases with the decreasing of the contact angle. The periods of the spreading and recoiling stages shorten with the increasing of the contact angle. In the cases of 30° and 60°, there is an oscillation after the recoiling. The spread factor becomes zero after recoiling in the cases of 90° and 120°. The reason is that the droplet re-bounces in these two cases. The

sequence of simulated results of 120° is shown in Fig.20. In the case of 150°, the droplet splashes after the impact. Tiny droplets are continuously ejected from the rim of the droplet. At last the main droplet itself re-bounces from the solid surface. The sequence of simulated results of 150° is shown in Fig.21. It is often reported that there exists a critical impact Weber number We_c of splashing. However, the Weber numbers in the above cases are the same and the only difference is the surface condition. This implies that the critical Weber number is dependent on the surface condition. This explains the widely scattered We_c reported in the literature. These phenomena are also in agreement with the observation of Šikalo et al (2002).

4   Conclusion

A fully Lagrangian particle method, MPS (Moving Particle Semi-implicit) method, is employed to analyze a liquid droplet colliding with a flat solid surface. The mathematical model involves gravity, viscosity and surface tension. The wettability is considered by the contact angle model and the non-slip condition. The particles in the contact line area are specially treated in the contact angle model. The model is validated by comparison with theoretical results.

The complete dynamic process of droplet impingement on the solid surface is simulated including the spreading and the recoiling after the impingement. The splashing or the re-bounding of the droplet occurs in some cases. The calculated results show that wettability significantly affects the dynamic process. The maximum spreading factor decreases with the increase of the contact angle. The splashing and the re-bounding of the drop are likely to occur in the cases of larger contact angle Therefore, the critical Weber numbers for splashing or re-bounding are not constant with respect to the wettability.

The two-dimensional model is employed in present study. The further work is to extent the present model to three-dimensional.

Reference

Andreaus, U.; Batra, R.C.; Porfiri, M. (2005):Vibrations of cracked Euler-Bernoulli beams using Meshless Local Petrov-Galerkin (MLPG) method. *CMES-Computer Modeling in Engineering & Sciences* 9, 111.

Atluri, S.N.; Liu, H.T.; Han, Z.D. (2006):Meshless Local Petrov-Galerkin (MLPG) mixed Finite Difference Method for solid mechanics. *CMES-Computer Modeling in Engineering & Sciences* 15, 1.

Bardenhagen, S.G.; Kober, E.M. (2004): The generalized interpolation material point method. *CMES-Computer Modeling in Engineering & Sciences* 5, 477.

Brackbill, J.U.; Kothe, D.B., Zemach, C. (1992): A continuum method for modeling surface tension. *J. Comput. Phys.* 100, 335.

Bussmann, M.; Chandra, S.; Mostaghimi, J. (1999): On a three-dimensional volume tracking model droplet impact. *Phys. Fluids* 11, 1406.

Bussmann, M.; Chandra, S.; Mostaghimi, J. (2000): Modeling the splash of a droplet impacting a solid surface. *Phys. Fluids* 12, 3121.

Ching, H.K.; Chen, J.K. (2006): Thermomechanical analysis of functionally graded composites under laser heating by the MLPG method. *CMES-Computer Modeling in Engineering & Sciences* 13, 199.

Cokmez-Tuzla, A.F.; Tuzla, K.; Chen, J.C. (2000): Characteristics of liquid-wall contact in post-CHF flow boiling. *Int. J. Heat Mass Transfer* 43, 1925.

Davies, J.T.; Rideal, E.K. (1961): Interfacial Phenomena. Academic Press Inc.(London), London, pp35.

Fukai, J.; Zhao, Z.; Poulikakos, D.; Megaridis, C.M.; Miyatake, O. (1993): Modeling of the deformation of a liquid droplet impinging upon a flat surface. *Phys. Fluids* A 5, 2588.

Fukai, J.; Shiiba, Y.; Yamamoto, T.; Miyatake, O.; Poulikakos, D.; Megaridis, C.M.; Zhao, Z. (1995): Wetting effects on the spreading of a liquid droplet colliding with a flat surface: Experiment and modeling. *Phys. Fluids* 7, 236.

Fukai, J.; Shiiba Y.; Miyatake, O. (1997): The-oretical study of droplet impingement on a solid surface below the Leidenfrost temperature. *Int. J. Heat Mass Transfer* 40, 2490.

Guo, Y.J.; Mishima, K. (2002): A non-equilibrium mechanistic heat transfer model for post-dryout dispersed flow regime. *Experimental Thermal and Fluid Science* 26, 861.

Guo, Y.J.; Nairn, J.A. (2006): Three-dimensional dynamic fracture analysis using the material point method. *CMES- Computer Modeling in Engineering & Sciences* 16, 141.

Harlow, F.H.; Shannon, J.E. (1967): The splash of a liquid droplet. *J. Appl. Phys.* 38, 3855.

Harlow, F.H.; Welch, J.E. (1965): Numeri-cal calculation of time-dependent viscous incom-pressible flow of fluid with free surface. *Phys. Fluids* 8, 2182.

Hirt, C.W.; Nichols, B.D. (1981): Volume of fluid (VOF) method for the dynamics of free boundaries. *J. Comput. Phys.* 39, 201.

Kang. B.S.; Lee, D.H. (2000): On the dynamic behavior of a liquid droplet impacting upon an in-clined heated surface. *Experiments in Fluids* 29, 380.

Kim, H.Y.; Chun, J.M. (2001): Recoiling of liq-uid droplets upon collision with solid surfaces. *Phys. Fluids* 13, 643.

Koshizuka, S.; Oka, Y. (1996): Moving-particle semi-implicit method for fragmentation of incom-pressible fluid. *Nucl. Sci. Eng.* 123, 421.

Liu, H.; Lavernia, E.J.; Rangel, R.H. (1993): Numerical simulation of substrate impact and freezing of droplets in plasma spray processes. *J. Phys. D: Appl. Phys.* 26, 1900.

Ma, J.; Liu, Y.; Lu, H.B. (2006): Multiscale sim-ulation of nanoindentation using the generalized interpolation material point (GIMP) method, dis-location dynamics (DD) and molecular dynamics (MD). *CMES- Computer Modeling in Engineer-ing & Sciences* 16, 41.

Nomura, K.; Koshizuka, S.; Oka, Y.; Obata, H. (2001): Numerical analysis of droplet breakup be-havior using particle method. *J. Nucl. Sci. Tech.* 38, 1057.

Pasandideh-Fard, M.; Bhola, R.; Chandra S.; Mostaghimi, J. (1998): Deposition of tin droplets on a steel plate: simulation and experiments. *Int. J. Heat Mass Transfer* 41, 2925.

Rein, M. (1993): Phenomena of liquid drop im-pact on solid and liquid surfaces. *Fluid Dyn. Res.* 12, 61.

Reznik, S.N.; Yarin, A.L. (2002): Spreading of an axisymmetric viscous drop due to gravity and capillarity o a dry horizontal wall. *Int. J. Multi-phase Flow* 28, 1437.

Riboo, R.; Marengo, M.; Tropea, C. (2002): Time evolution of liquid drop impact onto solid, dry surfaces. *Experiments in Fluids* 33, 112.

Roisman, I.V.; Rioboo, R.; and Tropea, C. (2002): Normal impact of a liquid drop on a dry surface: model for spreading and receding. *Proc. R. Soc.* Lond. A 456, 1411.

Slattery, J.C.; Flumerfelt, R.W. (1982): In-terfacial Phenomena. In: Hetsroni. G. (Ed.), Handbook of Multiphase Systems. Hemisphere, Washington and McGraw-Hill, New York Vol.1, Chap.4.

Sladek, J.; Sladek, V.; Zhang, C. (2006): Mesh-less local Petrov-Galerkin method for linear cou-pled thermoelastic analysis. *CMES–Computer Modeling in Engineering & Sciences* 16, 57.

Šikalo, Š.; Marengo, M.; Tropea, C.; Ganić, E.N. (2002): Analysis of impact of droplets on horizontal surfaces. *Experimental Thermal and Fluid Science* 25, 503.

Tang, Z.; Shen, S.; Atluri, S.N. (2003): Anal-ysis of materials with strain-gradient effects: A Meshless Local Petrov-Galerkin(MLPG) ap-proach, with nodal displacements only. *CMES-Computer Modeling in Engineering & Sciences* 4, 177.

Tong, A.Y.; Holt, B.R. (1997): Numerical study on the solidification of liquid metal droplets im-pacting onto a substrate. Numer. *Heat Transfer* A 31, 797.

Trapaga G.; Szekely, J. (1991): Mathematical modeling of the isothermal impingement of liquid droplets in spray processes. *Metall.Trans.* B. 22, 901.

Trujillo, M.F.; Lee, C.F. (2001): Modeling crown formation due to the splashing of a droplet. *Phys. Fluids* 13, 2503.

Worthington, A.M. (1877): On the forms assumed by drops of liquid falling on a horizontal plate. *Proc. R. Soc.* London 25, 261.

XIE, H.; Koshizuka, S.; Oka, Y. (2004a): Modeling of a single drop impact onto liquid film using particle method. *Int. J. Numer. Methods Fluids* 45, 1009.

XIE, H.; Koshizuka, S.; Oka, Y. (2004b): Numerical simulation of liquid drop deposition in annular-mist flow regime of boiling water reactor. *Journal of nuclear science and technology* 41 (5), 569.

XIE, H.; Koshizuka, S.; Oka, Y. (2005): Simulation of drop deposition process in annular mist flow using three-dimensional particle method. *Nuclear Engineering and Design* 235, 1687.

Yarin, A.L.; Weiss. D.A. (1995): Impact of drops on solid surfaces: self-similar capillary waves and splashing as a new type of kinematic discontinuity. *J. Fluid Mech.* 283, 141.

Zapałowicz, Z. (2002): Critical contact Weber number for toluene droplets dropping onto the heated wall surface. *Experimental Thermal and Fluid Science* 25, 523.

Zhang, Y.; Yabe, T. (1999): Effect of ambient gas on three-dimensional breakup in coronet formation. *CFD J.* 8, 378.

Zhao, Z.; Poulikakos,D.; Fukai, J. (1996a): Heat transfer and fluid dynamics during the collision of a liquid droplet on a substrate-I. Modeling. *Int. J. Heat Mass Transfer* 39, 2771.

Zhao, Z.; Poulikakos, D.; Fukai, J. (1996b): Heat transfer and fluid dynamics during the collision of a liquid droplet on a substrate-II. Experiments. *Int. J. Heat Mass Transfer* 39, 2791.